Journal of Power Sources 243 (2013) 654–660

Contents lists available at SciVerse ScienceDirect

Journal of Power Sources

journal homepage: www.elsevier.com/locate/jpowsour

Study of $Sr_2Mg(Mo_{0.8}Nb_{0.2})O_{6-\delta}$ as anode material for solid oxide fuel cells using hydrocarbons as fuel

M.J. Escudero [a,*], I. Gómez de Parada [a,b], A. Fuerte [a], L. Daza [a,c]

[a] Energy Department, CIEMAT, Av. Complutense 40, 28040 Madrid, Spain
[b] Faculty of Science, Autonomuous University of Madrid, Campus Cantoblanco, 28049 Madrid, Spain
[c] Insitute of Catalysis and Petrochemistry, CSIC, Campus Cantoblanco, C/ Marie Curie 2, 28049 Madrid, Spain

HIGHLIGHTS

- A single double perovskite phase was obtained in air and kept under reduction condition.
- Optimum catalytic properties for methane conversion under conditions of partial oxidation and combined reforming.
- Electrochemical studies revealed high tolerance to carbon deposition.

ARTICLE INFO

Article history:
Received 14 January 2013
Received in revised form
20 May 2013
Accepted 29 May 2013
Available online 13 June 2013

Keywords:
SOFC
Anode
Double perovskite
$Sr_2MgMoO_{6-\delta}$
Nb

ABSTRACT

$Sr_2Mg(Mo_{0.8}Nb_{0.2})O_{6-\delta}$ (SMMNb) was investigated as potential anode material of solid oxide fuel cells (SOFCs) for direct oxidation of methane. The compound was prepared by solid state reaction, followed by annealing under reducing atmosphere of 10% H_2/N_2 at 900 °C. The structural and morphological properties of fresh and reduced material were characterized by XRD, XPS and SEM. Additionally, catalytic properties towards oxidation of methane, electrical properties in reducing atmosphere as well as thermal and chemical compatibility with common SOFC electrolytes were investigated. These results reveal a double perovskite single phase in the fresh and reduced compound and, after reduction, a change in the niobium valence was observed. SMMNb shows a good activity for methane partial oxidation as well as combined reforming reaction. The material presents a semiconductor behaviour with *n*-type electronic conduction and an excellent thermal compatibility with SOFC electrolytes such as SDC, GDC and LSGM, based on similarity of values of TEC. However, this material reacts with zirconia-based electrolytes (YSZ and ScSZ). Although, a low electrochemical activity for H_2 and CH_4 oxidation was found, SMMNb demonstrates high tolerance to carbon deposition when the anode is exposed to methane.

1. Introduction

In the recent years, Solid Oxide Fuel Cells (SOFCs) have achieved a great deal of attention as a potential source of emission free energy for both small mobile auxiliary power as well as for megawatt scale stationary power [1]. One of the greatest advantages of a SOFC compared to most other fuel cell technologies is the possibility to use hydrocarbon fuels in addition to the more traditional hydrogen. The state-of-art SOFC with Ni-cermet anode shows high efficiency when hydrogen is used as fuel, but exhibits some severe problems when hydrocarbon fuels were used, such as poor redox stability, carbon deposition (coking) and sulphur poisoning, unless the fuel is desulphurized and reformed before use [2–4]. Thus, there is a great interest to find alternative anode materials for SOFC. Ceramic mixed ionic-electronic conductor (MIEC) materials have been identified as possible candidates to overcome many of the problems of the Ni-based anodes [2–4].

Many ceramics have been investigated as potential anode materials, most of them based on perovskite-type structure, such as chromium manganites derived from (La, Sr)$Cr_{0.5}Mn_{0.5}O_{3-\delta}$ [5,6], doped strontium titanium oxides [7–10] and double perovskites based on $SrMgMoO_{6-\delta}$ [11–15]. Theses anodes exhibit the ability to directly operate on hydrocarbon fuels without external reforming. Nevertheless, chromium manganites show a low performance for direct hydrocarbon oxidation while the activated titanates present limitations as low reduction kinetics and low electronic conductivity.

* Corresponding author. Tel.:+34 913466622; fax: +34 91346269.
E-mail address: m.escudero@ciemat.es (M.J. Escudero).

0378-7753/$ – see front matter © 2013 Elsevier B.V. All rights reserved.
http://dx.doi.org/10.1016/j.jpowsour.2013.05.198

However, Huang et al. [11,12] reported that the double perovskite $SrMgMoO_{6-\delta}$ yielded high power densities when using methane as a fuel, and a good tolerance to sulphur. Marrero-López et al. [16] and Bernuy-López et al. [17] further confirmed that this material displayed high redox stability at up to 1000 °C under 5% H_2/N_2 and 1200 °C under 5% H_2/Ar reducing conditions, respectively. Though, in a recent work Bi et al. [18] observed that $SrMgMoO_{6-\delta}$ possessed very poor intrinsic catalytic activity for oxidation of both H_2 and CH_4 in absence of Pt paste/mesh as anodic current collector. On the other hand, Vasala et al. [2] have investigated the substitution effects of the redox active element Mo in $SrMgMoO_{6-\delta}$ by W and Nb in the structure and electrical properties. They suggested that low substitution levels of Nb in $SrMgMoO_{6-\delta}$ could enhance the electrocatalytic oxidation activity due to an increase of ionic conductivity. In addition, niobium compounds are well known to show an excellent catalytic activity for different reactions, being used as active catalysts for methane oxidation [19].

Based on this context, in the present work, $Sr_2Mg(Mo_{0.8}Nb_{0.2})O_{6-\delta}$ (SMMNb) has been synthesized and explored as an alternative SOFC anode material for direct oxidation of methane. Its structure, catalytic activity, thermal expansion coefficient, morphology, electrical conductivity and chemical compatibility with common electrolytes in SOFC (YSZ, ScSZ, SDC, GDC and LSGM) have been studied. Its electrochemical oxidation of hydrogen and methane has also been investigated by impedance spectroscopy (IS) as function of temperature using symmetrical cell with LSGM as electrolyte.

2. Experimental

$Sr_2Mg(Mo_{0.8}Nb_{0.2})O_{6-\delta}$ oxide was synthesized by solid state reaction. Stoichiometric amounts of predried high purity $SrCO_3$, MgO, MoO_3 and Nb_2O_5 were mixed in acetone and then calcined in air at 1000 °C for 15 h. The resulting powder was subsequently ground in acetone in a zirconia ball mill for 4 h, and uniaxially pressed into pellets and sintered in air. SMMNb was fired at 1500 °C for 50 h. Reduced phases were obtained by further reduction at 900 °C under flowing 10% H_2/N_2 for 50 h.

X-ray powder diffraction (XRD) patterns were obtained using a PANalytical X'Pert Pro diffractometer, equipped with a Cu Kα (1.5406 Å) radiation source.

X-ray photoelectron spectra (XPS) were recorded with a Perkin–Elmer PHI 5400 spectrometer equipped with a Mg Kα excitation source ($h\nu$ = 1253.60 eV) and a beam size of 1 mm diameter. In order to take into account the charging effects on the measured binding energies, these energies were determined by referencing to the C 1s peak at 284.8 eV.

The morphology and chemical composition of the samples were examined with scanning electron microscopy (SEM) using a Hitachi microscope S-2500 combined with energy-dispersive X-ray spectroscopy (EDX), model Sun Sparcstation.

Thermogravimetric (TG) analyses were carried out in order to determine oxygen stoichiometry changes in the samples. The TG experiments were conducted on a Mettler Toledo TGA/SDTA 851e thermobalance. The calcined sample was heated to 1000 °C and cooled back to room temperature at a rate of 2 °C min^{-1} in 5% H_2/N_2 (50 ml min^{-1}).

Catalytic activity measurements for methane oxidation were tested in a tubular quartz reactor at atmospheric pressure from 400 to 800 °C. The catalyst bed was formed by 0.23 g of sample (0.25–0.42 mesh) and an inert diluter (SiC) in a 1/3 v/v. Prior to the catalytic measurements, the calcined sample was reduced *in situ* with 10% H_2/Ar mixture (50 ml min^{-1}) at room temperature up to 900 °C and isothermally kept at this temperature for 10 h. To assess the oxidation activities, two gas compositions were considered 5:2 CH_4:O_2 mixture for the partial oxidation condition and 5:2:0.6 CH_4:O_2:CO_2 mixture for combined reforming with a total flow rate of 50 ml min^{-1} (GHSV = 20,200 h^{-1}). Argon was used as the balance gas. Reaction products were analysed with a Varian 3400 chromatograph connected in line, equipped with a TCD detector and molecular sieve 13 Å and Porapak Q columns.

At the end of catalytic run, the sample was subjected to a temperature programmed oxidation (TPO) test in order to estimate the carbon deposition. TPO experiment was carried out in 10% O_2/Ar mixture (50 ml min^{-1}) from room temperature up to 1000 °C with a rate of 10 °C min^{-1} using a TG-DTA equipment. Gases evolution was analysed with a Pfeiffer Omnistar quadrupolar mass spectrometer.

Thermal expansion coefficients (TEC) were measured on an alumina dilatometer Linseis L75/1550, from room temperature to 1000 °C at a rate of 5 °C min^{-1} in both static air and 5% H_2/N_2.

The chemical reactivity of sample with commercial electrolytes such as 8% mol Y_2O_3 stabilised ZrO_2 (YSZ, Pikem), 10% mol ScO_3 stabilised ZrO_2 (ScSZ, Praxair), $Sm_{0.2}Ce_{0.8}O_{2-\delta}$ (SDC, Praxair), $Gd_{0.1}Ce_{0.9}O_{2-\delta}$ (GDC, Praxair) and $La_{0.9}Sr_{0.1}Ga_{0.8}Mg_{0.2}O_{3-\delta}$ (LSGM, Praxair) was investigated at 900 °C, in dry H_2 for 50, by combining in 1:1 weight ratio. After the chemical stability reaction the products were examined by XRD.

The electrical conductivity of the material was measured in 10% H_2/N_2 by the four point DC method in the temperature range 400–800 °C. The sample was previously reduced at 900 °C for 20 h under 10% H_2/N_2. The electrical contacts were ensured with gold wire and a gold conductor paste. A current load was applied by a Schlumberger Solartron 1286 Electrochemical Interface and the potential drop recorded by a Digital Multimeter (Agilent E34401A). High-temperature conductivity measurements as a function oxygen partial pressures, $p(O_2)$, from 10^{-23} to 10^{-17} atm were performed at 800 °C. The $p(O_2)$ values were monitored using a YSZ oxygen sensor placed next to the pellet in the cell.

The electrochemical characterization was carried out on symmetrical cell configuration with a superficial area of 0.65 cm^2 using LSGM as electrolyte. The dense electrolyte was obtained by pressing the commercial powders of LSGM under 3 ton uniaxial force to form a green pellet. After sintering, a dense LSGM pellet was obtained with a diameter of ~9 mm and a thickness of ~1.9 mm. Subsequently, a porous $La_{0.4}Ce_{0.6}O_{4-\delta}$ (LCD, Praxair) layer was deposited onto both sides of the dense electrolyte by tape casting using PMMA as pore former, and then annealing in air at 1400 °C for 2 h. A thin LDC buffer layer (≈100 μm thick) was used between the anode material and the electrolyte to prevent interdiffusion of ionic species between the perovskite anode and electrolyte [11]. SMMNb anode material was made into ink with a binder (Decoflux, WB41, Zschimmer and Schwartz). SMMNb ink was screen-printed onto both sides of LCD porous, following by firing at 1000 °C in air for 2 h. The resulting electrodes were 60 μm thick. Finally, Au current collector was placed on anode material using Au ink, and fired at 900 °C for 2 h.

The anode activity over the electrolytes was evaluated by the interfacial area specific resistance (ASR) in the described symmetrical cell configuration by electrochemical impedance spectroscopy, in wet H_2 and CH_4, as temperature function (600–800 °C). Humidified hydrogen and/or methane were supplied to the symmetrical cell as fuel at a flow rate of 50 ml min^{-1}, after passing through a saturator at room temperature to adjust the gas humidity at 3% H_2O. The impedance spectra were collected by an AUTOLAB system (PGSTAT30 and FRA2 module) from Eco Chemie B.V. The measurements were performed from 100 KHz to 10 mHz at open circuit with a signal amplitude of 5 mV. Zview software was used to fit the experimental data to the equivalent circuits. All impedance data were normalized by the superficial area so they are given in Ω cm [2] units and divided by 2 since the cell is symmetrical.

3. Results and discussion

Fig. 1 shows the XRD patterns of SMMNb sample before and after reduction at 900 °C in dry 10% H_2/N_2 for 50 h. Spectra reveals the formation of a single phase double perovskite structure after sintering in air at 1500 °C and no impurity phases were detected, such as $SrMoO_4$. Note that $SrMoO_4$ phase is a common impurity in this kind of materials when they are synthesized in air [2,9,16]. So, it might be concluded that the presence of Nb as well as the higher synthesis temperature hinders its formation. The single phase double perovskite structure without impurity phase was kept after reduction.

XPS analyses were used to study the chemical state of the Mo and Nb elements and their content in the compound. The XPS spectra of Mo 3d and Nb 3d for the air calcined and reduced SMMNb powders are illustrated in Fig. 2. All high resolution Mo 3d spectra exhibit doublet (Mo $3d_{5/2}$ and Mo $3d_{3/2}$) with asymmetrical peaks. The two spectra of Mo for air synthesized and reduced SMMNb are practically identical indicating that Mo does not suffer important variations under reduction conditions (Fig. 2a). The deconvoluted peaks (not shown) revealed two doublets located at 230.8 and 233.9 eV and 232.2 and 235.5 eV. These spectral lines are assigned to Mo $3d_{5/2}$ and Mo $3d_{3/2}$, peaks of Mo^{5+} and Mo^{6+} states, respectively [16]. The molar percentage of Mo^{5+} and Mo^{6+} estimated were 6.2% and 93.8%, respectively for air synthesized sample and 8.7% and 91.3% after its exposure in H_2. Then, the XPS results indicate that the average composition of Mo does not significantly change due to the reduction treatment.

The Nb 3d core level spectra present two peaks that correspond to the doublets Nb $3d_{5/2}$ and Nb $3d_{3/2}$ (Fig. 2b). Initially, the Nb 3d signal exhibits two peaks centred at 206.6 ($3d_{5/2}$) and 209.3 ($3d_{3/2}$) eV. After its exposure in H_2, it can be observed a shift of these peaks towards lower binding energies, 205.9 and 208.7 eV, which indicates a lower oxidation state of niobium. According to the literature [20], curve fitting of the Nb 3b spectrum for oxidized sample yields two components Nb^{5+} and Nb^{4+}, their binding energies are 206.4 and 205.1 eV for the Nb-$3d_{5/2}$ peak and 209.1 and 207.8 eV for the Nb-$3d_{3/2}$ peak, respectively. The ion concentration extracted from the fitting curve is 85.7% for Nb^{5+} and 16.3% for Nb^{4+}. While, the reduced SMMNb were satisfactory fitted to one doublet, indicating that niobium is presented only in an oxidation state of 4.

The above mentioned XPS analysis revealed that the incorporation of niobium in the structure stabilizes Mo^{6+}, whereas, after reduction treatment the Nb is reduced but Mo does not change its oxidation state.

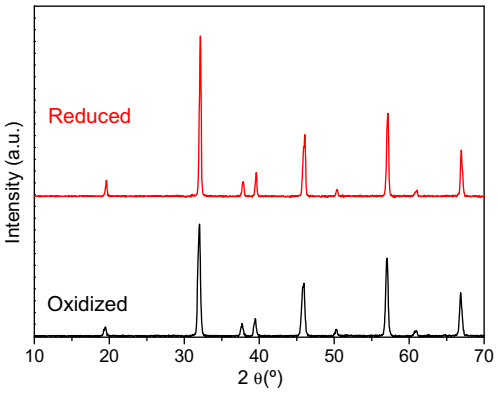

Fig. 1. XRD patterns of SMMNb sample synthesized in air and reduced at 900 °C in dry 10% H_2/N_2 for 50 h.

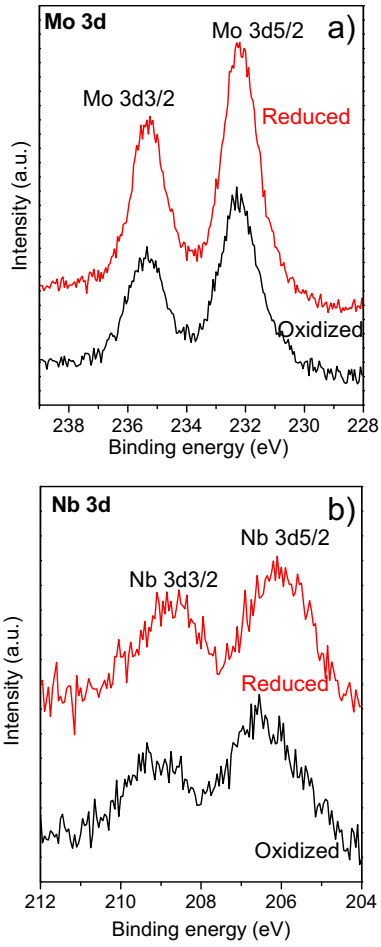

Fig. 2. XPS spectra of SMMNb before and after its reduction in 10% H_2/N_2 for 50 h; a) Mo 3d core level region; b) Nb 3d core level region.

Related with the morphology of SMMNb, it is very similar after air calcination or reduction treatment (Fig. 3). The samples exhibit an inhomogeneous particle size distribution with formation of agglomerates with an average grain size about 0.2–2 μm. EDX microanalysis was performed on eight surface points of sample before and after reduction. All EDX spectra indicated only the constituent elements of Sr, Mg, Mo, Nb and O, and revealed that the average atomic concentrations are 2.11 (Sr), 0.89 (Mg), 0.81 (Mo) and 0.19 (Nb). The experimental values are in good agreement with the nominal ones, showing that the stochiometric index $Sr_2MgMo_{0.8}Nb_{0.2}O_{6-\delta}$ oxide was obtained and kept the same composition after reduction.

The redox stability of air-calcined sample was studied by thermogravimetry. Sample was reduced in 5% H_2/Ar at 1000 °C and then cooled down in air, at room temperature, with a heating rate of 2 °C min^{-1}. It was observed a small weight loss of 2.4%. This change corresponds to an escape of oxygen from the lattice, which gives rise to oxygen vacancies probably due to the reduction of Nb^{5+} to Nb^{4+}, as XPS results confirmed. During the cooling period, no significantly weight changes were observed.

In the SOFC anode operating environment, oxygen is transported from the cathode to the anode under polarization. Although passing gas mixture over a catalytic bed does not exactly replicate the anodic condition but it is perhaps the best approximation than can be achieved. The catalytic activity of SMMNb sample for methane oxidation was investigated as function of temperature

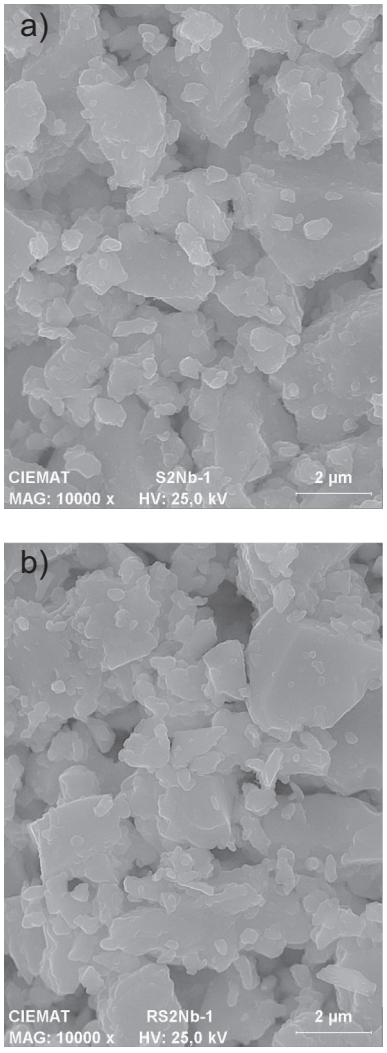

Fig. 3. SEM micrographs of SMMNb: a) synthesized in air; b) reduced at 900 °C in dry 10% H_2/N_2 for 50 h.

from 400 to 800 °C. Previous to the catalytic activity tests, different residence times as well as stoichiometries of gas mixture were tested to select the conditions to perform the methane oxidation using SMMNb as catalyst. The selected conditions were as follow: $W/F = 8$ g h mol^{-1}, total flow rate = 50 ml min^{-1} and 5:2 CH_4:O_2 gas stream composition. Blank tests were carried out filling the reactor only by SiC to avoid hot spots under the same experimental conditions. No reactions were detected in the gas phase below 700 °C, whereas a methane conversion of 1.4% was achieved at 800 °C. Blank test results are included in Fig. 4. Fig. 4a shows the steady state curved obtained by 5:2 CH_4:O_2 gas mixture on sample. The reaction starts at 550 °C and the oxidation products are CO_2, H_2, CO and H_2O. Methane conversion increased with the temperature and reached 17.2% at 800 °C. Notice that oxygen was entirely consumed by methane at 750 °C, with a maximum methane conversion by oxidation reaction of 16.5% (after subtraction of the reaction blank).

CO_2 reforming is relevant for SOFC operations, where a fraction of the CO_2 product could be recycled along with the natural gas feed. To investigate the influence of CO_2 on the oxidation reaction of methane as function of temperature it was added to the 5:2 CH_4:O_2 gas mixture, the final gas composition of 5:2:0.6 CH_4:O_2:CO_2 was used (Fig. 4b). It can be observed that the curves follow the same steady-state trend as that obtained under methane oxidation

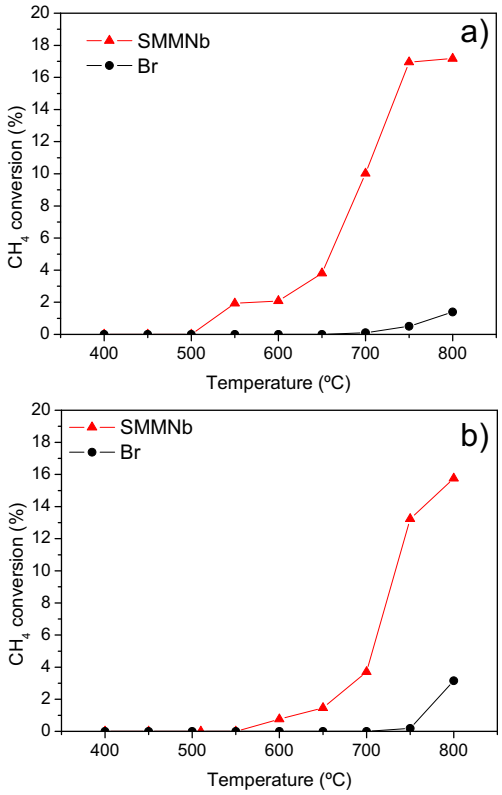

Fig. 4. Methane conversion on SMMNb as a function of temperature for gas mixtures: a) 5:2 CH_4:O_2.; b) 5:2:0.6 CH_4:O_2:CO_2. (Br) represents the blank reactor.

conditions (5:2 CH_4:O_2), although a slightly higher light-off temperature was observed for combining-reformed conditions. No significant influence on the methane conversion over SMMNb was detected in the presence of CO_2. The maximum of methane conversion reached at 800 °C was 15.8% and 3.1% for blank reactor. This suggested a low CO_2 reforming ability of this material.

After cooling the reactor, no carbon deposition was visually observed over sample. To investigate the possible carbon formation, temperature programmed oxidation (TPO) studies were conducted at the end of catalytic reactions. This analysis (Fig. 5) revealed very low carbon coverage on both post-reaction samples. It can be observed three peaks of CO_2, two peaks around 300, 400 and 750 °C that correspond to different types of carbon deposits. According to bibliography, the carbon atoms oxidized at 750 °C are

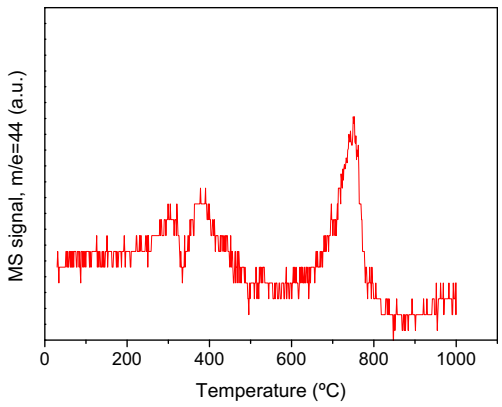

Fig. 5. Evolution of CO_2 during TPO tests performed over SMMNb sample.

related to graphitic films and the carbon oxidized at lower temperature (300–500 °C) are associated to amorphous filaments or films [21].

Another aspect to taking into consideration is the thermal expansion coefficients of the SOFC component materials; the incompatibility between then causes excessive thermal stress, which leads to the cracking and mechanical failure of the multi-layer and hence reduces the lifetime of the SOFCs or even break the single cells [14]. The thermal expansion of SMMNb were measured in air and 5% H_2/N_2 in the temperature range of 200–1000 °C, curves presented a gradual increase as the temperature increased (Fig. 6). The thermal expansion depends on the electrostatic forces within the lattice, which depend on the concentration of positive and negative charges and their distances within the lattice. The thermal expansion increases if the attractive forces decrease. All expansion curves are linear indicating that there is not structural phase transition in the studied temperature range. The average thermal expansion coefficients of compound, obtained from the slope of the line in the temperature range 200–1000 °C, were 13.7×10^{-6} and $14.6 \times 10^{-6}\ K^{-1}$ under air and 5% H_2/N_2, respectively. The reduction atmosphere yields an increase in the oxygen vacancy concentration which produces larger TEC value. These results are in agreement with the oxygen loss calculated from TG analyses, and XRD and XPS results. These TEC values are closed to those for YSZ, ScSZ, SDC, GDC and LSGM (10.5×10^{-6}, 11.9×10^{-6}, 12.3×10^{-6}, 12.9×10^{-6} and $11.8 \times 10^{-6}\ K^{-1}$, respectively), electrolytes commonly used in SOFC.

So important as a good thermal compatibility is the chemical compatibility of electrode materials with electrolyte that is a prerequisite any further cell testing. An excessive phase reaction between the electrolyte and the electrode might create new phases or even ionically insulating layer, which can increase the ohmic resistance of the cell and block the oxygen transference affecting the cell performance. In this sense, reactivity studies were carried out to assess the interaction between SMMNb material and five different standard electrolytes: YSZ, ScSZ, SDC, GDC and LSGM. The XRD patterns of the different SMMNb-electrolyte powders mixtures fired at 900 °C for 50 h under 10% H_2/N_2 are shown in Fig. 7. The XRD patterns of electrolytes obtained in the same conditions are also included for comparison.

There is an obvious reaction of SMMNb with zirconia-based electrolytes which is more significantly with YSZ (Fig. 7a). The reactivity study between SMMNb and YSZ or ScSZr revealed the corresponding cubic phase for YSZ or cubic and rhombohedral phases coexist for ScSZ [22], and double perovskite phase together with new impurity peaks that were assigned to $SrZrO_3$ and MgO. Consequently, the high reactivity between anode materials studied and zirconia-based electrolytes (YSZ and ScSZ) limited their combined use in a SOFC without a protective layer to prevent reaction. Furthermore, no diffraction peak around 27.6° was observed,

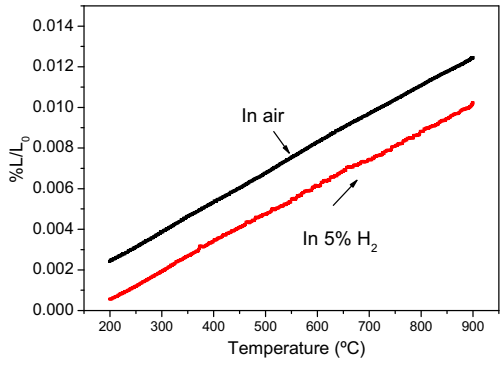

Fig. 6. Thermal expansion curves of SMMNb in air and in 5 %H_2/N_2.

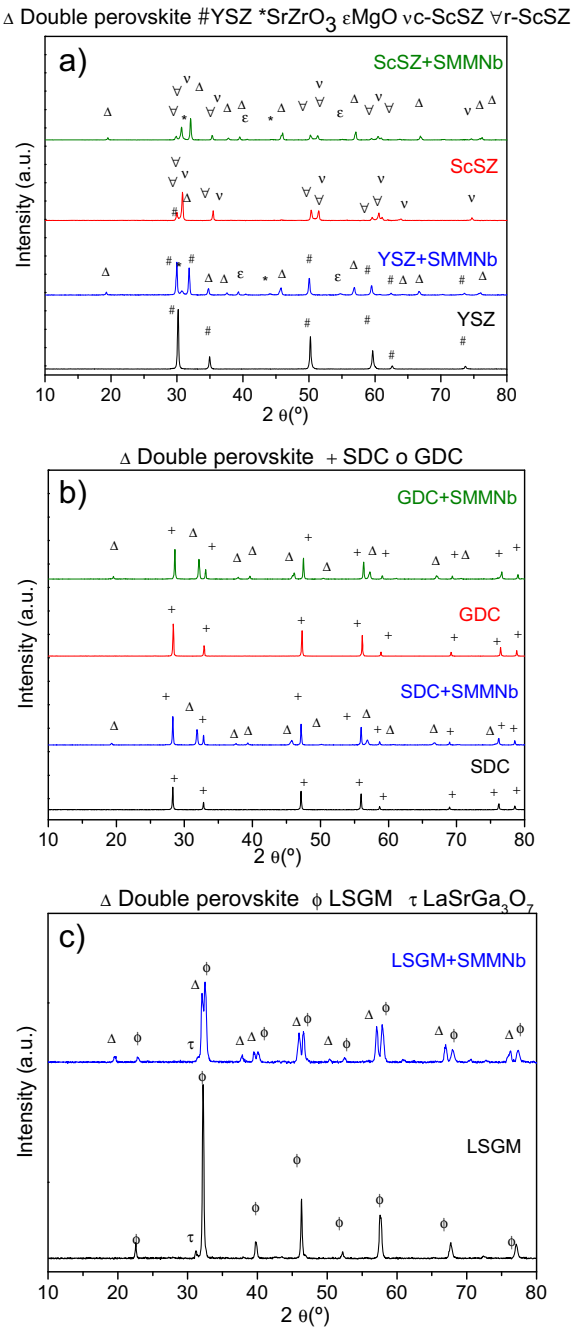

Fig. 7. XRD patterns for chemical compatibility tests between SMMNb samples and five different standard electrolytes: a) YSZ and ScSZ; b) SDC and GDC; c) LSGM.

indicating the absence of $SrMoO_4$ phase. The formation of this impurity has been previously observed in chemical reactivity test between Sr_2MgMoO_6 and YSZ electrolyte [16]. As mentioned before for fresh sample, the presence of niobium in the composition has inhibited its formation once again.

No impurity peaks were detected for mixtures SMMNb with ceria-based (SDC and GDC) or LSGM electrolytes. As can be seen in Fig. 7b and c, diffraction peaks attributed to double perovskite appear together with those for cubic fluorite phases of cerium-doped oxide or cubic perovskite phase and secondary phase of $LaSrGa_3O_7$ for LSGM. $LaSrGa_3O_7$ is one of the major impurities in doped gallates [23], and presents a low conductivity compared to LSGM. Then, its presence in the electrode/electrolyte interface

could deteriorate the fuel cell performance. It should be noted that $LaSrGa_3O_7$ phase appears in the XRD pattern of fresh LSGM electrolyte so it could be concluded that it is not a product of reaction between electrode and electrolyte. Therefore, the results indicate a good chemical compatibility for both studied materials with ceria-based and LSGM electrolytes at 900 °C.

On the other hand, the electrical conductivity of reduced SMMNb was measured in dry 10% H_2/N_2 by four-terminal DC point in the temperature range of 400–800 °C (Fig. 8a). The electrical conductivity enhances with increasing of temperature with a maximum conductivity value of 0.2 S cm^{-1} at 800 °C. Vasala et al. [2] also observed that the Nb substitution for Mo in $SrMgMoO_{6-\delta}$ reduced the electrical conductivity and obtained values of 2.1 and 0.6 S cm^{-1} at 800 °C in 5% H_2/Ar for SMM and SMMNb, respectively. This value is higher than that measured here, but in the same order of magnitude. The difference in conductivity values could be explained by the different synthesis conditions employed.

Fig. 8b shows the electrical conductivity measured in 10% H_2/N_2 with leaking air at 800 °C as function of oxygen partial pressure pO_2 in the range 10^{-21}–10^{-13} atm. With increasing pO_2 the conductivity decreases, indicative of an *n*-type conductivity as the dominant electronic mechanism.

As can be seen in Fig. 8a, Arrhenius plots displayed a strictly linear relationship, exhibiting a semiconductive behaviour. The temperature dependence of the conductivity can be described by the small polaron hopping mechanism:

$$\sigma = \frac{A}{T}\exp\left(-\frac{E_a}{kT}\right) \quad (1)$$

where A is the pre-exponential constant, k is the Boltzmann constant, T is the absolute temperature, and E_a is activation energy of the electrical conductivity. The activation energy (E_a) was calculated from the slope of the curve of log (σT) vs 1000 T^{-1}, as shown in Fig. 8a, which yielded value of 0.75 eV. At low pO_2, charge compensation is achieved by the formation of vacancies due to Nb^{5+} is reduced to lower valence states. Thus, the concentration of oxygen vacancies expected to increase under reducing conduction, which in turn will increase the oxide-ion conductivity. In addition, an increase of temperature enhances the conductivity due to the activation of lattice oxygen.

In the case of SMMNb, the activation energy is higher than 0.197 or 0.255 eV for $Sr_2MgMoO_{6-\delta}$ reported by Huang [11] and Marrero-López [16], respectively, which could indicate a change in the conductivity mechanism. The substitution of Nb for Mo in $Sr_2MgMoO_{6-\delta}$ could increase the amount of oxygen vacancies in the lattice that enhances its ionic conductivity and/or stabilize to Mo^{6+} ions, reducing the amount of the Mo^{5+}/Mo^{6+} redox couple which decreases the electronic conduction. According the XPS results, under reduction condition niobium is only present as Nb^{4+} then only Mo shows mixed valence. The ionic conduction in these materials is assumed to be orders of magnitude lower than the electronic conduction [16].

Finally, the electrochemical study was carried out. Impedance spectra for SMMNb electrode with LSGM as electrolyte were measured using a symmetrical cell configuration in wet H_2 and CH_4 as function of temperature (600–800 °C). Previously, in order to study the stability of the system, the cell was reduced at 900 °C for 10 h in 10% H_2(dry) and then impedance measurements were carried out previously and after 100 h of exposure under this atmosphere at 800 °C. As can be seen in Fig. 9, similar Nyquist diagrams were obtained what suggests that the materials are stable under this condition.

Fig. 10 shows the impedance spectra obtained for the SMMNb/LSGM interfaces at 800 °C in the aforementioned gas compositions. All impedance data have been normalized to get area specific resistance value. It can be seen that the lowest impedance values were obtained in wet H_2 as fuel.

All experimental data were analysed, using the Zview software (Scribner Associate). The best equivalent circuit fitting comprises a series of the three parallel combinations of resistance and a constant phase element. The process of electrochemical oxidation of fuel in anode/electrolyte interface usually possesses three different contributions. The high frequency arc is usually attributed to the transfer of species charges trough the anode/electrolyte interface. The intermediate frequency arc is usually associated to the charge transfer reaction, whereas the low frequency arc is usually ascribed to diffusion process or/and adsorption of charged species [24]. In all cases, the highest resistance values were ascribed at the arc at low

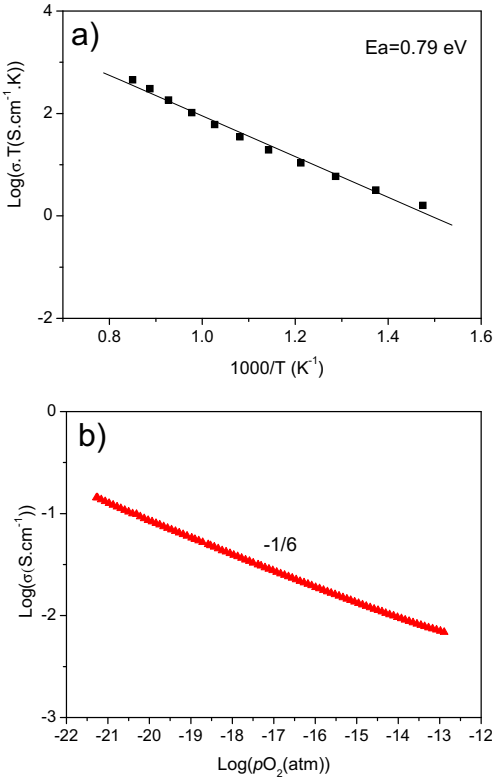

Fig. 8. Electrical conductivity for SMMNb: a) Arrhenius plot in 10% H_2/N_2; b) as function of oxygen partial pressure at 800 °C.

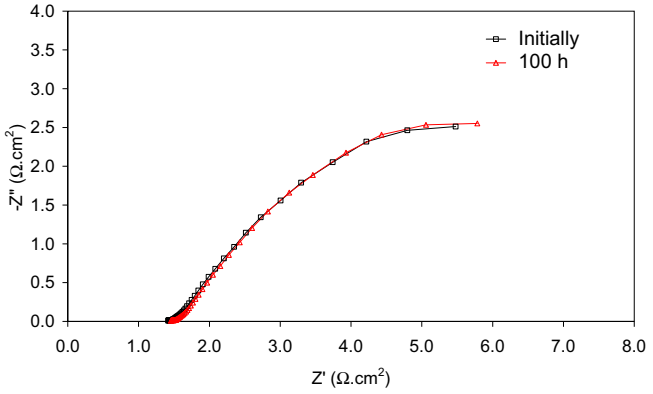

Fig. 9. Electrochemical studies of SMMNb/LSGM interface in 10% H_2/N_2 at 800 °C as function of time.

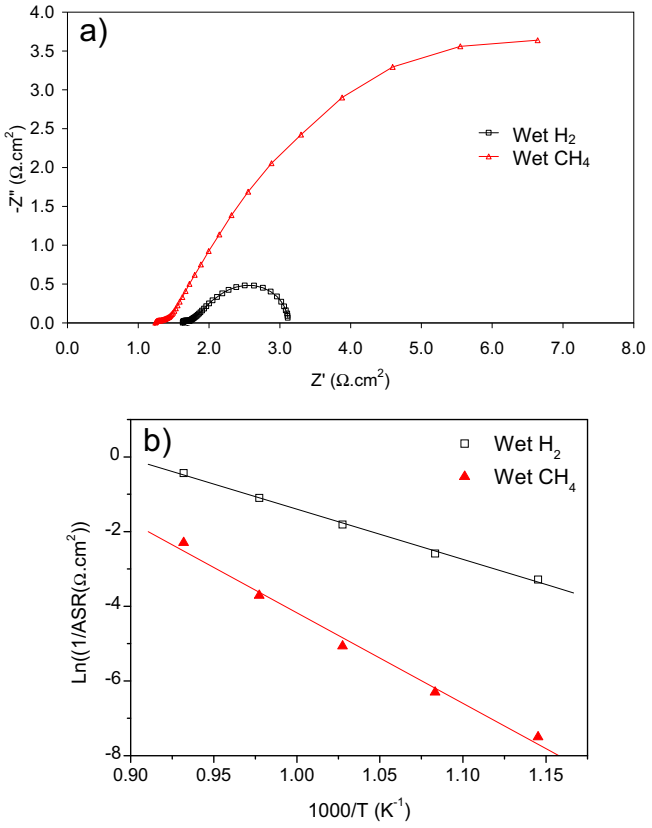

Fig. 10. Electrochemical studies of SMMNb/LSGM interface in wet H_2 and CH_4: a) Impedance spectra at 800 °C; b) Arrhenius plots of the ASR values from 600 to 800 °C.

frequency associated with high capacitance values (0.2–2 F cm^{-2}) that could be indicate the adsorption of charged species as the limiting step for the oxidation of hydrogen or methane reactions. The area specific resistance (ASR) was obtained by the sum of the individual resistance of the three arcs involved in the fitting. The ASR values are directly depending on the rate limiting step of the electrochemical process involved in the fuel oxidation reaction at the anode.

Fig. 10b shows the Arrhenius plots of the ASR values of the SMMNb/LSGM interface in the temperature range of 600–800 °C in wet H_2 and CH_4. The electrode polarization was a thermally activated phenomenon with activation energy (E_a) around of 1.16 and 2.28 eV in wet H_2 and CH_4, respectively. The higher ASR values and E_a obtained in methane could be due to a competitive adsorption between the carbonous species as CO, CO_2 or C and other species that limit the fuel oxidation process. After the electrochemical measurements of SMMNb in wet CH_4, at first sight, no carbon deposition was detected on the anode, which indicates that SMMNb does not support methane cracking to a large extent. Therefore, this oxide should show high resistance to carbon deposition.

4. Conclusions

$Sr_2Mg(Mo_{0.8}Nb_{0.2})O_{6-\delta}$ has been examined with respect to its structural, catalytic and electrochemical properties towards oxidation of methane in the context of its potential application as anode for SOFC. A well-defined structure of single phase double perovskite was obtained in air and kept under reduction conditions. XPS data revealed that the molybdenum valence does not show a significantly change after the reduction treatment and the niobium coexists as Nb^{4+} and Nb^{5+} in the air sintered sample and only as Nb^{4+} after its reduction. The compound reached at 800 °C a maximum methane conversion of 16.5 and 12.7% for partial oxidation and combined reforming conditions, respectively. TEC values of SMMNb are 13.5 × 10^{-6} K^{-1} in air and 14.6 × 10^{-6} K^{-1} in 5% H_2/N_2, which are close to that of common SOFC electrolytes. The compound shows a good chemical compatibility with SDC and GDC and LSGM electrolytes and high reactivity with YSZ and ScSZ although the reaction is most severe with YSZ. The reduced sample exhibits a semiconductor behaviour with an Ea of 0.75 eV and the maximum electrical conductivity value was of 0.2 S cm^{-1} at 800 °C in dry 10% H_2. Its electrical conductivity drops with increasing pO_2 values indicating *n*-type electronic conduction. The electrochemical studies revealed that the low frequency process related to adsorption of hydrogen or carbonous species as CO, CO_2 or C and other species on SMMNb surface could be the limiting process for oxidation reaction of hydrogen or methane. The SMMNb/LSGM interface shows the best performance at 800 °C with ASR of 3.1 Ω cm^2 and 11.7 Ω cm^2 under H_2 and CH_4, respectively.

Acknowledgements

This work was supported by Spanish Ministry of Economic and Competitiveness (MAT2010-20846) and the Community of Madrid (DIVERCEL; Ref.S009/ENE-1475).

References

[1] P. Gansor, C. Xu, K. Sabolsky, J.W. Zondlo, E.M. Sabolsky, J. Power Sources 198 (2012) 7–13.
[2] S. Vasala, M. Lehtimäki, S.C. Haw, J.M. Chen, R.S. Liu, H. Yamauchi, M. Karppinen, Solid State Ionics 181 (2010) 754–759.
[3] J.B. Goodenough, Y.H. Huang, J. Power Sources 173 (2007) 1–10.
[4] C. Sun, U. Stimming, J. Power Sources 171 (2007) 247–260.
[5] S. Tao, J.T.S. Irvine, J. Electrochem. Soc. 151 (2) (2004) A252–A259.
[6] X.C. Lu, J.H. Zhu, Solid State Ionics 178 (2007) 1467–1475.
[7] O.A. Marina, N.L. Canfield, J.W. Stevenson, Solid State Ionics 149 (2002) 21–28.
[8] H. Kurokawa, L. Yang, C.P. Jacobson, L.C. De Jonghe, S.J. Visc, J. Power Sources 164 (2007) 510–518.
[9] X. Huang, H. Zhao, W. Qiu, W. Wu, X. Li, Energy Convers. Manage. 48 (2007) 1678–1682.
[10] S. Hui, A. Petric, J. Electrochem. Soc. 149 (2002) J1–J10.
[11] Y.H. Huang, R.I. Dass, J.C. Denyszyn, J.B. Goodenoughz, J. Electrochem. Soc. 157 (7) (2006) A1266–A1272.
[12] Y.H. Huang, R.I. Dass, Z.L. Xing, J.B. Goodenoughs, Science 312 (2006) 254–257.
[13] Y.H. Huang, G. Liang, M. Croft, M. Lehtimäki, M. Karppinen, J.B. Goodenough, Chem. Mater. 21 (2009) 2319–2326.
[14] Z. Wang, Y. Tian, Y. Li, J. Power Sources 196 (2011) 6104–6109.
[15] P. Zhang, Y.H. Huang, J.G. Cheng, Z.Q. Mao, J.B. Goodenough, J. Power Sources 196 (2011) 1738–1743.
[16] D. Marrero-López, J. Peña-Martínez, J.C. Ruiz-Morales, D. Pérez-Coll, M.A.G. Aranda, P. Nuñez, Mater. Res. Bull. 43 (2008) 2441–2450.
[17] C. Bernuy-López, M. Allix, C.A. Bridges, J.B. Claridge, M.J. Rosseinsky, Chem. Mater. 19 (2007) 1035–1043.
[18] Z.H. Bi, J.H. Zhu, J. Electrochem. Soc. 158 (6) (2011) B605–B613.
[19] K. Tanabe, Catal. Today 78 (2003) 65–67.
[20] P.C. Karulkar, J. Vac. Sci. Technol. 18 (2) (1981) 169–174.
[21] J. Sfeir, P.A. Buffat, P. Möckli, N. Xanthopoulos, R. Vasquez, H.J. Mathieu, J. Van Herle, K.R. Thampi, J. Catal. 202 (2001) 229–244.
[22] T. Shimonosono, H. Kimura, Y. Saca, J. Ceram. Soc. Jpn. 118 (2010) 1038–1043.
[23] K. Huang, J.H. Wan, J.B. Goodenough, J. Electrochem. Soc. 148 (7) (2001) A788–A794.
[24] I.S. Primdah, M. Mogensen, J. Electrochem. Soc. 144 (1997) A1547–A1553.